Observation of Direct Processes in Photoproduction at HERA

ZEUS Collaboration

November 15, 1993

Abstract

Jets in photoproduction events have been studied with the ZEUS detector for γp centre-of-mass energies ranging from 130 to 250 GeV. The inclusive jet distributions give evidence for the dominance of resolved photon interactions. In the di-jet sample the direct processes are for the first time clearly isolated. Di-jet cross sections for the resolved and direct processes are given in a restricted kinematic range.

1 Introduction

Electron proton scattering is dominated by the exchange of almost real photons. Although most of the photoproduction cross section is due to soft processes, a fraction of the γp collisions at HERA energies is expected to contain high-p_T processes. In lowest-order QCD, these hard processes are of two main types [1, 2], as shown in figure 1. In the *direct* processes, the photon participates as a point-like particle, interacting with a gluon ($\gamma g \to q\bar{q}$, photon gluon fusion) or a quark ($\gamma q \to gq$, QCD Compton scattering). In the *resolved* processes, the photon behaves as a source of partons which can scatter off those in the proton. The unscattered constituents of the photon then give rise to a hadronic system, known as the photon remnant, going approximately in the direction of the original photon.

Hard scattering in photoproduction should produce multi-jet structures with features similar to those observed in hadron-hadron collisions [3]. QCD-based models of these processes, including parton distributions in the photon and proton compatible with experimental data, predict that the resolved processes should dominate over the direct for a wide range of jet transverse energy [2, 4]. The presence of hard scattering in γp collisions has already been observed at HERA [5, 6], with evidence for multi-jet structures and for the presence of the resolved contribution.

In this study, we have searched for jets in a sample of photoproduction events having a total transverse energy of at least 10 GeV. We demonstrate that the resolved processes form the majority of the events. Using a sample of di-jet events, we separate unambiguously for the first time the resolved and direct contributions and obtain cross sections for the two processes in a restricted kinematic region.

2 Experimental Setup

The main components of the ZEUS detector [5, 7] used in this analysis are the high resolution uranium-scintillator calorimeter (CAL), the central tracking detector and the luminosity monitor. The calorimeter covers the polar angle range between $2.6° < \theta < 176.1°$, where $\theta = 0°$ is the proton beam direction. It consists of three parts: the rear calorimeter (RCAL), covering the backward pseudorapidity [1] range ($-3.4 < \eta < -0.75$); the barrel calorimeter (BCAL) covering the central region ($-0.75 < \eta < 1.1$); and the forward calorimeter (FCAL) covering the forward region ($1.1 < \eta < 3.8$). The calorimeter is segmented in depth into electromagnetic (EMC) and hadronic (HAC) sections. The EMC sections are divided into cells of transverse dimensions 5×20 cm^2 (10×20 cm^2 in RCAL) and the HAC sections consist of cells of transverse dimension 20×20 cm^2. The energy resolution as measured under test beam conditions is $\sigma_E/E = 0.18/\sqrt{E}$ (E in GeV) for electrons and $\sigma_E/E = 0.35/\sqrt{E}$ for hadrons [8]. The timing resolution of the calorimeter cells, $\sigma_t = 1.5/\sqrt{E} \oplus 0.5$ ns [8, 9], allows rejection of out-of-time beam-gas interactions. In the analysis presented here calorimeter cells with EMC (HAC) energy below 60 MeV (110 MeV) are excluded to minimise the effect of calorimeter noise. This noise is dominated by uranium activity and has an r.m.s. value below 19 MeV for EMC cells and below 30 MeV for HAC cells. The central tracking detector [10] was used to measure charged

[1] $\eta = -\ln(\tan\frac{\theta}{2})$

particle trajectories in order to reconstruct a z vertex for each event, where the z-axis is defined to be along the direction of the proton beam.

To measure the luminosity, two lead-scintillator electromagnetic calorimeters were installed in the HERA tunnel [11]. One of these measures the electron energy and the other the photon energy for the bremsstrahlung process ($ep \to ep\gamma$). The electron calorimeter is also used to tag a fraction of very low photon virtuality (Q^2) events. These events have a Q^2 below 0.02 GeV^2 and will be referred to as 'tagged events' throughout the following. Events tagged in the luminosity monitor have γp centre-of-mass energies between 130 GeV and 280 GeV.

Data were collected during 1992, when 820 GeV protons were colliding with 26.7 GeV electrons. Collisions took place between nine electron and proton bunches. Non-colliding bunches of electrons and protons allowed an estimation of beam associated backgrounds. A three-stage trigger was in operation at ZEUS. At the first level, events were triggered by a minimum energy deposit in the CAL [7]. The rejection of beam-gas interactions was achieved using timing information from scintillator counters near the beams at the first level trigger and from the calorimeter at the second and third levels.

3 Data Selection Criteria

The raw data sample used in this analysis consists of about four million events, corresponding to an integrated luminosity of 25.5 nb^{-1}. The analysis follows the data selection described in reference [5]. A first filter required a trigger signal in the electromagnetic sections of the BCAL or RCAL and either of the following two conditions: 1) more than 10 GeV energy deposited in the FCAL and more than 2.5 GeV deposited in the RCAL or 2) more than 20 GeV total energy and more than 10 GeV total transverse energy deposited in the whole calorimeter. About 350,000 events satisfied these conditions. In order to reduce the proton beam-gas contamination, a more refined second filter was applied. Firstly, it was required that all events should have a reconstructed vertex. Secondly, stringent requirements on the timing as measured by the CAL and on the correlation between the z-vertex position and the event time measured in the FCAL [12] were applied with negligible loss of genuine ep events.

In order to select a sample of photoproduction events, deep inelastic neutral current events were removed as follows. Electron candidates were identified using the pattern of energy distribution in the calorimeter. For events with an electron candidate, the inelasticity parameter, y, was calculated from the electron variables:

$$y_e = 1 - \frac{E'_e}{2E_e}(1 - \cos\theta'_e).$$

where E_e, E'_e and θ'_e are the incident electron energy and the energy and angle of the scattered electron, respectively. For photoproduction events with $Q^2 = 0$, y is equal to the ratio of the photon energy to the electron beam energy. A number of photoproduction events have electron candidates found in the calorimeter. These are hadrons misidentified as electrons, or genuine electrons which are not the scattered beam electron. Generally for these events the calculated value of y_e is high. Therefore, in order to minimise the loss of photoproduction events from the sample, an event is rejected only if y_e is less than 0.7. The cut is very effective in removing deep inelastic events with $Q^2 > 4$ GeV^2.

Further suppression of the background from beam-gas collisions and the contamination from deep inelastic interactions was achieved using y estimated from the calorimeter energy using the Jacquet-Blondel [13] formula

$$y_{JB} = \frac{\Sigma_i (E - p_z)_i}{2E_e}$$

where the sum runs over all calorimeter cells i and p_z is the z-component of the momentum vector assigned to each cell of energy E. This formula is valid under the assumption that the scattered electron escapes down the beam pipe. The cell angles are calculated from the geometric centre of the cell and the vertex position of the event. Final state particles produced close to the direction of the proton beam give a negligible contribution, since these particles have $(E - p_z) \sim 0$. Events in the range $0.2 < y_{JB} < 0.7$ are selected. The lower cut suppresses background due to proton beam-gas collisions. Remaining deep inelastic events are removed by the higher cut since y_{JB} will be incorrectly measured to be ~ 1 for these events, due to the presence of the scattered electron in the calorimeter. Finally, events were selected with a total transverse energy deposition in the calorimeter in excess of 10 GeV.

After these cuts 19,589 events remained. The beam-gas contamination was estimated from the non-colliding bunches to be at most 0.3%. The contamination from cosmic rays was estimated to be at most 0.1%. The contamination from deep inelastic events with $Q^2 > 4$ GeV^2 was estimated to be $< 0.5\%$ using Monte Carlo techniques.

The γp centre-of-mass energy (W) of these events can be calculated via the expression $W \approx \sqrt{4 y_{JB} E_e E_p}$, where E_p is the proton energy. In the final sample W ranges from 130 GeV to 250 GeV. For events tagged by an electron in the range 5 GeV $\leq E'_e \leq$ 25 GeV (5390 out of the 19,589) a comparison of the W measured from the electron energy and from the hadronic system showed for the latter a systematic underestimation of approximately 10%. This discrepancy is attributed to energy losses in inactive material in front of the CAL and to particles lost in the rear beam pipe, and is adequately reproduced in the Monte Carlo simulation of the detector.

To ensure that the data are photoproduction events, the mean value of Q^2 in the sample was estimated. This was done using the Monte Carlo simulation, since the scattered electron escapes undetected (except for tagged events) down the beam pipe, and the Q^2 resolution from the measured transverse energy in the central detector is insufficient. A Monte Carlo simulation for the direct processes (see below) gives a mean value of 0.03 GeV^2 and produces the same fraction of tagged events (for which the Q^2 is below 0.02 GeV^2) as in the data. The mean Q^2 is expected to be similar for the resolved processes.

4 Monte Carlo Simulation

Two independent Monte Carlo generators, HERWIG5.7 [14] and PYTHIA5.6 [15], were used to simulate the hard photoproduction processes. In these generators, the direct and resolved processes are each simulated using leading order matrix elements, with the inclusion of initial and final state parton showers. The lower cut-off on the transverse momentum of the generated final-state partons ($p_{T\,min}$) was chosen to be 2.5 GeV/c [14, 16].

Fragmentation into hadrons is performed using a cluster algorithm in HERWIG and a LUND string model in PYTHIA. The lepton-photon vertex is modelled according to the Weizsäcker–Williams approximation, except in the case of the simulation of the direct processes in HERWIG where exact matrix elements are used.

Events were generated using the leading order prediction by GRV [17] for the photon and MRSD0 [18] for the proton parton distributions. In addition, samples of events using DG [19] and LAC1 [20] for the photon and MRSD$^-$ for the proton parton distributions were studied.

The generated events were passed through detailed detector and trigger simulation programs based on the GEANT package [21]. They were reconstructed using standard ZEUS off-line programs and passed through the same analysis chain as the data.

5 Analysis of Jet Production

We searched for jet structure in the selected data sample using a jet finding algorithm in pseudorapidity (η) - azimuth (ϕ) space [22, 23]. The cone radius $R = \sqrt{\Delta\phi^2 + \Delta\eta^2}$ in the algorithm was 1 unit. This value was chosen in order to contain the relatively low transverse momentum jets studied here. Calorimeter cells within 10° ($\eta > 2.44$) of the proton beam direction were excluded from the jet analysis. Remnants of the proton are expected to be predominantly at angles below this value. Cells were grouped into clusters; those clusters with transverse energy (E_T^{jet}) larger than 5 GeV were called jets. Below this value the sensitivity to the $p_{T\,min}$ cut in the Monte Carlo simulations becomes large. The transverse momentum weighted mean pseudorapidity (η^{jet}) and azimuth (ϕ^{jet}) of each jet were evaluated and jets were accepted for the present analysis if η^{jet} was less than 1.6 ($\theta > 22.8°$). This cut was dictated by the chosen value of R and the need to remove calorimeter cells near the proton beam direction.

Of the sample of 19,589 events, 6.5%, 1.4% and 0.1% of the events were of the one-jet, two-jet and three-jet type, respectively. A total of 1548 events with jets was found. From a comparable number of Monte Carlo events, a QCD based simulation using the HERWIG generator predicts the fractions to be in the range 6.3-9.8% and 0.7-1.9% for the one-jet and two-jet categories, respectively. The quoted ranges indicate the spread of the values obtained with the different proton and photon parton distributions mentioned above. The agreement between data and Monte Carlo simulation for the jet multiplicities is also good if the radius of the cone is set to 0.7 units. The fraction of three-jet events in the Monte Carlo sample, which does not include higher order matrix elements, was 0.01%.

The inclusive jet sample consists of 1850 jets. The E_T^{jet} distribution, shown in figure 2a, falls steeply, reaching values as high as 18 GeV. It should be noted that the data in this and subsequent figures are not corrected for energy absorbed in inactive material nor for resolution smearing and other detector effects. These effects are included in the Monte Carlo simulation. Only statistical errors are quoted in the figures. The Monte Carlo distribution (normalised to the data) for HERWIG is shown as a full line. The shape of the data is described well. The expected relative contributions of direct and resolved photon processes are also shown.

Figure 2b shows the inclusive η^{jet} distribution, together with the Monte Carlo distribution from HERWIG. Also shown for the Monte Carlo simulation are the separate contributions from resolved and direct processes. Since only a fraction of the photon's momentum participates in

the hard scatter in the resolved case, the centre of mass is in general more strongly boosted in the proton direction, and the two contributions have quite different η^{jet} distributions. The data require a substantial resolved component. The data show a rise of the jet rate towards high η^{jet} values which is not well reproduced by the Monte Carlo simulations. It is not clear whether this excess is due to an incorrect description of the proton remnant region or to the choice of parton distributions. In fig. 2b the Monte Carlo distribution is normalised to the number of jets in the data excluding the highest η^{jet} bin.

Di-jet production has been studied by selecting events with two or more jets in the accepted rapidity range ($\eta^{jet} \leq 1.6$). In the case of events with more than two jets the two jets with highest E_T^{jet} are taken as these are expected to most closely reflect the kinematics of the final state partons in leading order QCD. The di-jet sample consists of 284 events. The di-jet invariant mass (M^{jj}) spectrum, shown in figure 3a, extends up to values of 40 GeV. The E_T^{jet} spectrum of the di-jet sample, which reaches values as high as 18 GeV, is shown in figure 3b. The jet pseudorapidity distribution is shown in figure 3c. In all cases, the data and Monte Carlo distributions are in reasonable agreement. In particular the agreement extends to the highest pseudorapidity bin. Figure 3c shows again the need for a large contribution from resolved processes.

Further insight into the mechanism of di-jet production is gained by studying the scattering angle distribution, $cos\theta^*$. The angle θ^* is computed in the centre-of-mass frame of the two jets, with respect to the proton momentum boosted into the same frame. The angular distribution is displayed in figure 3d. The transverse momentum cut on the jets decreases the acceptance for events with low M^{jj} and high $\cos\theta^*$. In order to reduce the effect of this cut, events with $M^{jj} > 16$ GeV have been selected. The distribution rises at large values of $\cos\theta^*$; the drop beyond $\cos\theta^* = 0.8$ is an artifact resulting from the η^{jet} region selected. Below this value the $\cos\theta^*$ distribution reflects the angular distributions of the parton-parton scattering processes. The QCD-based simulations again acceptably reproduce the data.

Summarizing this section, these results show for several independent distributions agreement of the data with QCD simulations which include hard processes involving the partonic content of the photon. The same conclusions are reached using the PYTHIA Monte Carlo and other parameterisations of the proton ($MRSD^-$) and photon (DG and LAC1) parton distributions.

6 Observation of the Direct Component

In this section we use the selected di-jet sample to separate the contributions of the direct and resolved photon processes.

In two-to-two parton scattering, the momenta of the incoming partons can be calculated from the two partons in the final state. Let x_γ and x_p be the fractions of the photon and proton momenta carried by the initial-state partons (see figure 1). Conservation of energy and momentum gives

$$x_p = \frac{\sum_{partons}(E + p_z)_{parton}}{2E_p},$$

$$x_\gamma = \frac{\sum_{partons}(E - p_z)_{parton}}{2E_\gamma},$$

where E_γ is the initial photon momentum and the sum is over the two final state partons. For the direct processes, $x_\gamma = 1$.

The jet energies and momenta may be used to estimate the energies and momenta of the final state partons. Using the energy of the cells assigned to the jet to evaluate the jet energy and longitudinal momentum and since $E_\gamma \approx E_e y \approx E_e y_{JB}$, we can approximate x_p and x_γ as

$$x_p^{meas} = \frac{\sum_{jets}(E + p_z)_{jet}}{2E_p},$$

$$x_\gamma^{meas} = \frac{\sum_{jets}(E - p_z)_{jet}}{\sum_i (E - p_z)_i},$$

where the sum in the denominator runs over all calorimeter cells. Note that in the formula for x_γ^{meas} many systematic uncertainties in the measurement of energy by the calorimeter cancel out.

From Monte Carlo studies it is found that imposing the requirements $|\eta^{jet_1} - \eta^{jet_2}| \leq 1.5$ and $|\phi^{jet_1} - \phi^{jet_2}| > 120°$ improves the x_γ^{meas} resolution and these cuts are applied in the following analysis. The number of events surviving these cuts is 193. The contamination from deep inelastic interactions with $Q^2 \geq 4$ GeV^2 is evaluated to be at the 1-2% level. No events from the non-colliding bunches remain in this sample and visual scanning shows that no cosmic ray events remain in our final sample.

The distribution of x_p^{meas} is shown in figure 4a. From the Monte Carlo simulation, the estimated error in $\log x_p^{meas}$ is $\pm 24\%$ for resolved events and $\pm 9\%$ for direct events. The data range from 1.6×10^{-3} to 10^{-1} with a mean value of 1.4×10^{-2}. The Monte Carlo distributions describe the data well and are insensitive to the choice of proton parton distributions, since most of the range covered by the present data is in the region where precise measurements of the proton structure exist ($x_p^{meas} > 10^{-2}$). These measurements are well described by the parameterisations of the proton structure used here.

The x_γ^{meas} distribution shown in figure 4b rises at both low and high values. The Monte Carlo simulations of the resolved and direct processes, shown in the same figure, have very different characteristics. The resolved processes show a rise towards low x_γ^{meas} , as observed in the data, but cannot account for the rise at high x_γ^{meas} . This is the case for both HERWIG and PYTHIA and for all the parton distributions studied. The direct processes predict a sharp rise towards high x_γ^{meas} as observed in the data and only a small number of events for $x_\gamma^{meas} < 0.7$. For the Monte Carlo simulation of the resolved processes, the distribution of $(x_\gamma^{meas} - x_\gamma)$ peaks at around 0.1 (0.2) and has a width of 0.14 (0.22) for HERWIG (PYTHIA). We conclude that the peak at the high end of the x_γ^{meas} distribution cannot be reproduced from resolved processes by experimental and acceptance effects, and that this peak results from direct processes.

The sample of 44 tagged events, which have $Q^2 < 0.02$ GeV^2, also exhibit a peak in the high x_γ region. For this subsample of events we can also use the measurement of the scattered electron energy to calculate the photon energy and so obtain an alternative estimate of x_γ. The distribution thus obtained again peaks at the high values where the direct processes are expected.

In figure 4b the sum of the independently normalised contributions from the resolved and direct processes was fitted to the x_γ^{meas} distribution using the shapes predicted by Monte Carlo simulation. The combined fit is able to reproduce the data acceptably, although at low x_γ^{meas} there is a discrepancy related to jets in the most forward region. From the fit we obtain a contribution of 65±17 events from the direct processes. We subtract this number from the total 193 events in the sample, and attribute all the remaining events to resolved interactions. This is done to reduce possible bias due to the poor agreement between the resolved Monte Carlo distribution and the data at low x_γ.

7 Determination of Direct and Resolved Cross Sections

The clear separation between resolved and direct contributions allows us to measure the di-jet cross sections for each of the two processes. Extrapolation into kinematic regions not covered by the data sample depends heavily on the details of the Monte Carlo and parton distributions used, and this is particularly true for the resolved component. For this reason we give ep cross sections restricted to a kinematic region similar to that defined by the cuts used in the analysis.

From the full Monte Carlo sample, generated over the complete y range, we calculate the number of reconstructed di-jet events, N_{rec}, using the full detector simulation and including the experimental trigger conditions and the complete set of selection cuts used in the data analysis. Also from the full Monte Carlo sample, events with a generated y in the range 0.2 - 0.7 were selected. Using the generated momenta of the final state particles, two jets with transverse energies above 5 GeV and pseudorapidities below 1.6 were also required. These cuts select N_{gen} events and define the kinematic region of the quoted cross sections. The ratio N_{rec}/N_{gen} is the experimental di-jet acceptance. In this way the effects of the $|\phi_1^{jet} - \phi_2^{jet}|$ and $|\eta_1^{jet} - \eta_2^{jet}|$ cuts are also corrected.

The acceptance is determined separately for the direct and resolved processes. The numbers of direct and resolved events seen in the data are then divided by the product of the respective acceptance and the experimental luminosity to give di-jet cross sections within the defined kinematic region. The acceptances are around 25% for both the resolved and direct components and depend only weakly on the Monte Carlo simulation used and on x_γ^{meas}.

A study of possible systematic errors in the cross section measurements, arising from uncertainties in the fit and the acceptance calculations, has been carried out separately for the resolved and direct contributions. In all cases the uncertainties in the resolved and direct contributions are similar, and the larger of the two is quoted. The principal sources of possible errors are as follows: different proton and photon parton distributions give a systematic error of ± 12%. Different Monte Carlo generators (HERWIG and PYTHIA) give variations of ± 16% in the calculated cross sections. The sensitivity of our measurement to the $p_{T\,min}$ cut off in the Monte Carlo was investigated and gives an estimated uncertainty of ± 8%. The variation between different implementations of the jet finding algorithm and treatments of jet merging is ± 13%. The uncertainty in the absolute energy scale of the detector gives rise to a systematic error of ± 17%. The effect of uncertainty in the trigger threshold energies is ± 5%. Finally, a ± 5% uncertainty in the luminosity determination [12] is included in both calculations. The final results are 21.1 ± 5.2(stat.) ± 5.7(syst.) nb for the resolved contribution to the di-jet cross section and 9.4 ± 2.7(stat.) ± 2.7(syst.) nb for the contribution of the direct processes.

The quoted cross sections are the averages of the values obtained with different parton distributions, different Monte Carlo generators and different jet finding procedures mentioned above. These are cross sections for ep collisions with $Q^2 \approx 0$ leading to events in the kinematic region $0.2 \leq y \leq 0.7$ with two jets of transverse energies greater than 5 GeV and pseudorapidities below 1.6. The sum of the resolved and direct ep cross sections quoted here corresponds to around 1% of the total low-Q^2 ep cross section in the given y range.

The shapes of the distributions obtained using simulations based on leading order QCD are in acceptable agreement with the data. In order to obtain agreement with the measured cross section, the predictions for both the resolved and direct contributions have to be scaled up by factors of 1.3 to 1.8, depending upon the Monte Carlo simulation and parton distributions used. However, the ratio of the measured cross sections for resolved and direct processes is consistent with the leading order QCD predictions as described in the Monte Carlo.

8 Summary

A sample of hard quasi-real photoproduction events with centre-of-mass energies between 130 GeV and 250 GeV has been isolated in ep collisions at HERA. Jet structure is observed and analysed. The jet distributions are adequately described by Monte Carlo simulations involving resolved and direct processes, with the resolved processes being dominant.

In the di-jet sample the distribution of x_γ^{meas} , the measured fraction of the photon energy participating in the hard collision, shows a clear peak at large values. This is an unambiguous signature for the presence of direct processes. Fits to this distribution allow a separation and determination of the resolved and direct contributions. Di-jet ep cross sections involving the exchange of almost real photons in the region defined by $0.2 \leq y \leq 0.7$, jets with transverse energies greater than 5 GeV and pseudorapidities less than 1.6 are measured to be $21.1 \pm 5.2(\text{stat.}) \pm 5.7(\text{syst.})$ nb for the resolved and $9.4 \pm 2.7(\text{stat.}) \pm 2.7(\text{syst.})$ nb for the direct processes.

Acknowledgements

We thank the DESY Directorate for their strong support and encouragement. The remarkable achievements of the HERA machine group were essential for the successful completion of this work, and are gratefully appreciated.

References

[1] J. F. Owens, Phy. Rev. D21 (1980) 54.

[2] M. Drees and F. Halzen, Phys. Rev. Lett. 61 (1988) 275;
M. Drees and R.M. Godbole, Phys. Rev. D39 (1989) 169 and Bombay preprint BU-TH-92/5;
G. A. Schuler and T. Sjöstrand, Phys. Lett. B300 (1993) 169.

[3] See for example Proton Antiproton Collider Physics, edited by G. Altarelli and L. Di Lella (World Scientific Singapore, 1989)

[4] G. Kramer and S.G. Salesch in Proc. of the Workshop on Physics at HERA, DESY (1991) 649 and in DESY preprint, DESY-93-10;
L.E. Gordon and J.K. Storrow, Phys. Lett. B291 (1992) 320;
D. Bödeker, Phys. Lett. B292 (1992) 164;
M. Greco and A. Vicini, Frascati preprint, LNF-93/017 (April 1993).

[5] ZEUS Collaboration, M. Derrick et al., Phys. Lett. B297 (1992) 404.

[6] H1 Collaboration, T. Ahmed et al., Phys. Lett. B297 (1992) 205;
H1 Collaboration, I. Abt et al., Phys. Lett. B314 (1993) 436.
H1 Collaboration, presented by M. Erdmann at the XXVIIIth Rencontres de Moriond, Les Arcs, France, March 1993 and preprint DESY 93-077.

[7] ZEUS Collaboration, M. Derrick et al., Phys. Lett. B293 (1992) 465; ibid. B303 (1993) 183.

[8] ZEUS Calorimeter group, A. Andresen et al., Nucl. Inst. and Meth. A309 (1991) 101;
A. Bernstein et al., Nucl. Inst. and Meth. A336 (1993) 23;
U. Mallik et al., Proc. Int. Conf. on Calorimetry in High Energy Physics, FNAL (1990).

[9] A. Caldwell et al., Nucl. Inst. and Meth. A321 (1992) 352; see also A. Caldwell, talk given at the Int. Conf. on High Energy Physics at Dallas and L. Hervas, Thesis, Universidad Autónoma de Madrid, unpublished.

[10] N. Harnew et al., Nucl. Inst. and Meth. A279 (1989) 290;
C.B. Brooks et al., Nucl. Inst. and Meth. A283 (1989) 477;
B. Foster et al., Nucl. Phys. B (Proc. Suppl.) 32 (1993) 181.

[11] J. Andruszków et al., DESY 92–066 (1992).

[12] ZEUS Collaboration, M. Derrick et al., Phys. Lett. B315 (1993) 481.

[13] F. Jacquet and A. Blondel, Proc. of the Study for an *ep* Facility for Europe, ed. U. Amaldi, DESY 79/48 (1979) 391.

[14] G. Marchesini et al., Comp. Phys. Comm. 67 (1992) 465.

[15] H.-U. Bengtsson and T. Sjöstrand, Comp. Phys. Comm. 46 (1987) 43; T. Sjöstrand, CERN-TH.6488/92.

[16] G. Abbiendi, private communication.

[17] M. Glück, E. Reya and A. Vogt, Phys. Rev. D46 (1992) 1973.

[18] A. Martin, W.J. Stirling and R.G. Roberts, Phys. Rev. D47 (1993) 867.

[19] M.Drees and K.Grassie, Z. Phys. C28 (1985) 451.

[20] H. Abramowicz, K. Charchula and A. Levy, Phys. Lett. B269 (1991) 458.

[21] R. Brun et al., GEANT3, CERN DD/EE/84-1 (1987).

[22] UA1 Collaboration., G. Arnison et al., Phys. Lett. 123B (1983) 115.

[23] J. Huth et al., Proc. of the 1990 DPF Summer Study on High Energy Physics, Snowmass, Colorado, edited by E.L. Berger (World Scientific, Singapore,1992) p. 134.

Figure 1: Schematic diagrams showing examples of (a) a direct process and (b) a resolved process.

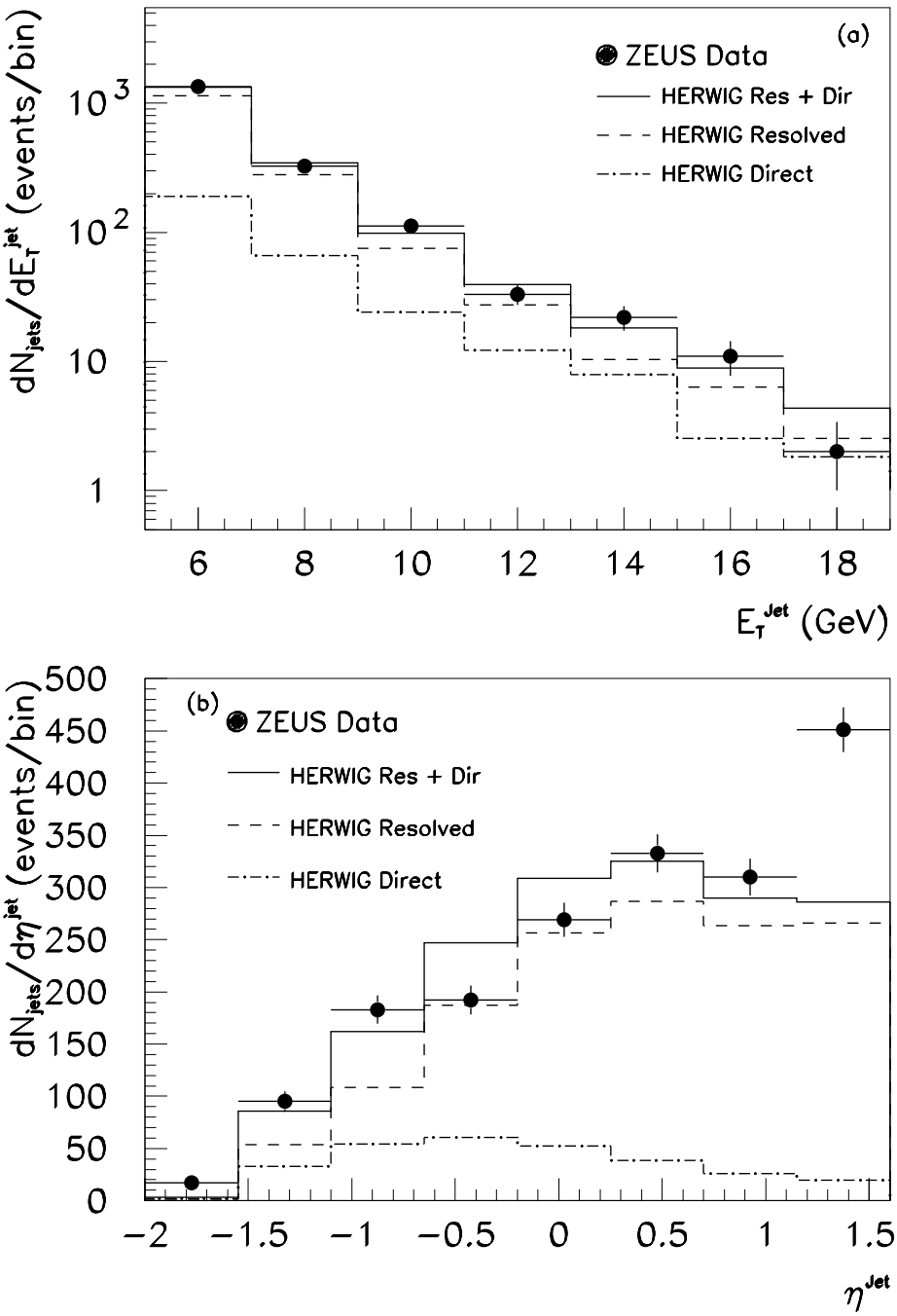

Figure 2: Inclusive jet distributions for (a) transverse energy of jets, (b) pseudorapidity of jets, where the Monte Carlo distribution is normalised to the data in the region $\eta^{jet} < 1.2$, as discussed in the text. The relative contributions of the direct and resolved processes as predicted by the Monte Carlo simulation are also shown.

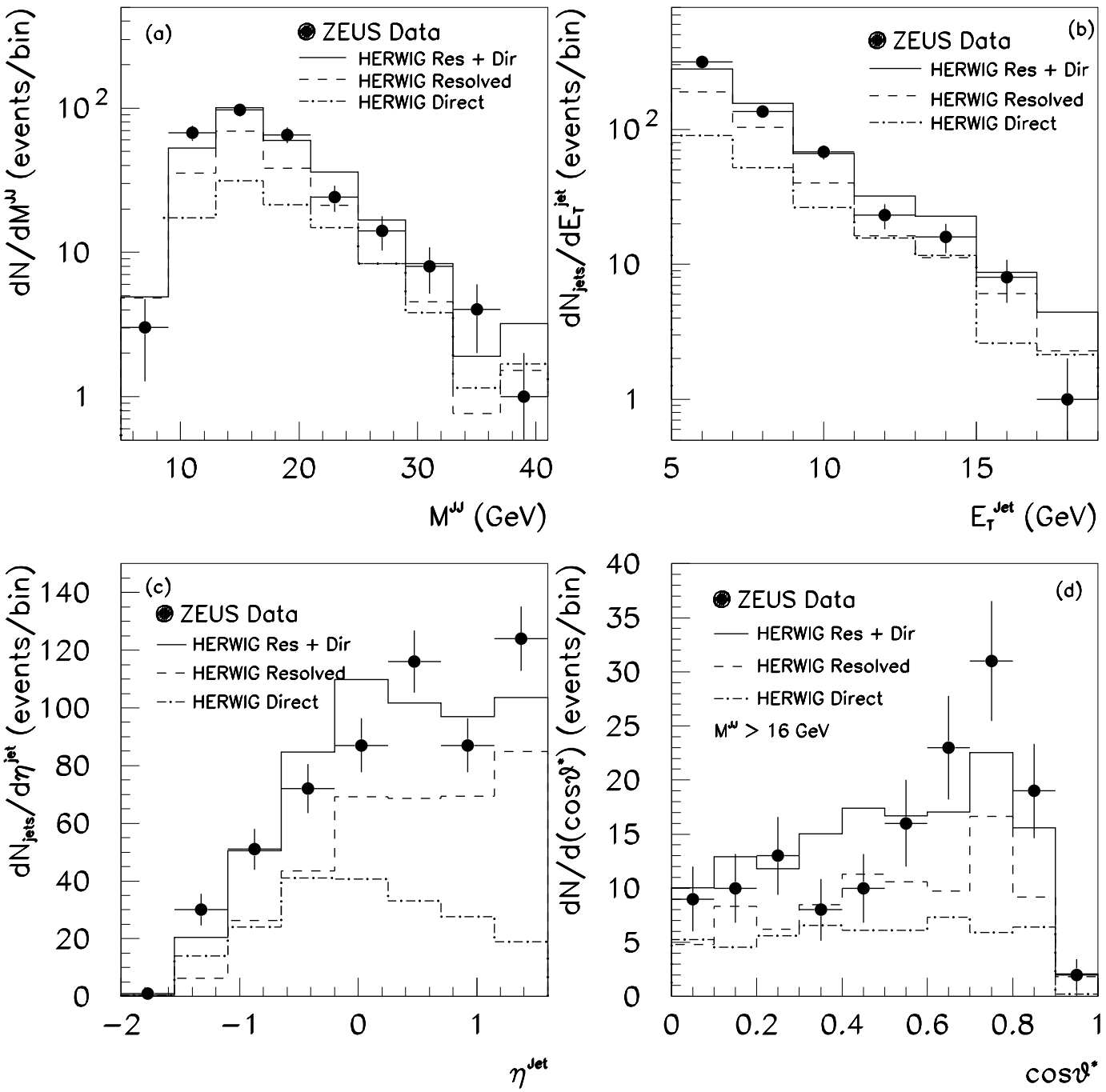

Figure 3: Kinematic distributions for events with two or more jets. The Monte Carlo is normalised to the data, and in all cases the relative contributions of the direct and resolved processes, as predicted by the Monte Carlo simulation, are shown. (a) Jet-jet invariant mass for jet pairs. (b) Transverse energy of jets. (c) Pseudorapidity of jets. (d) $\cos\theta^*$ of jet angles in the jet-jet c.m.s. measured with respect to the proton momentum.

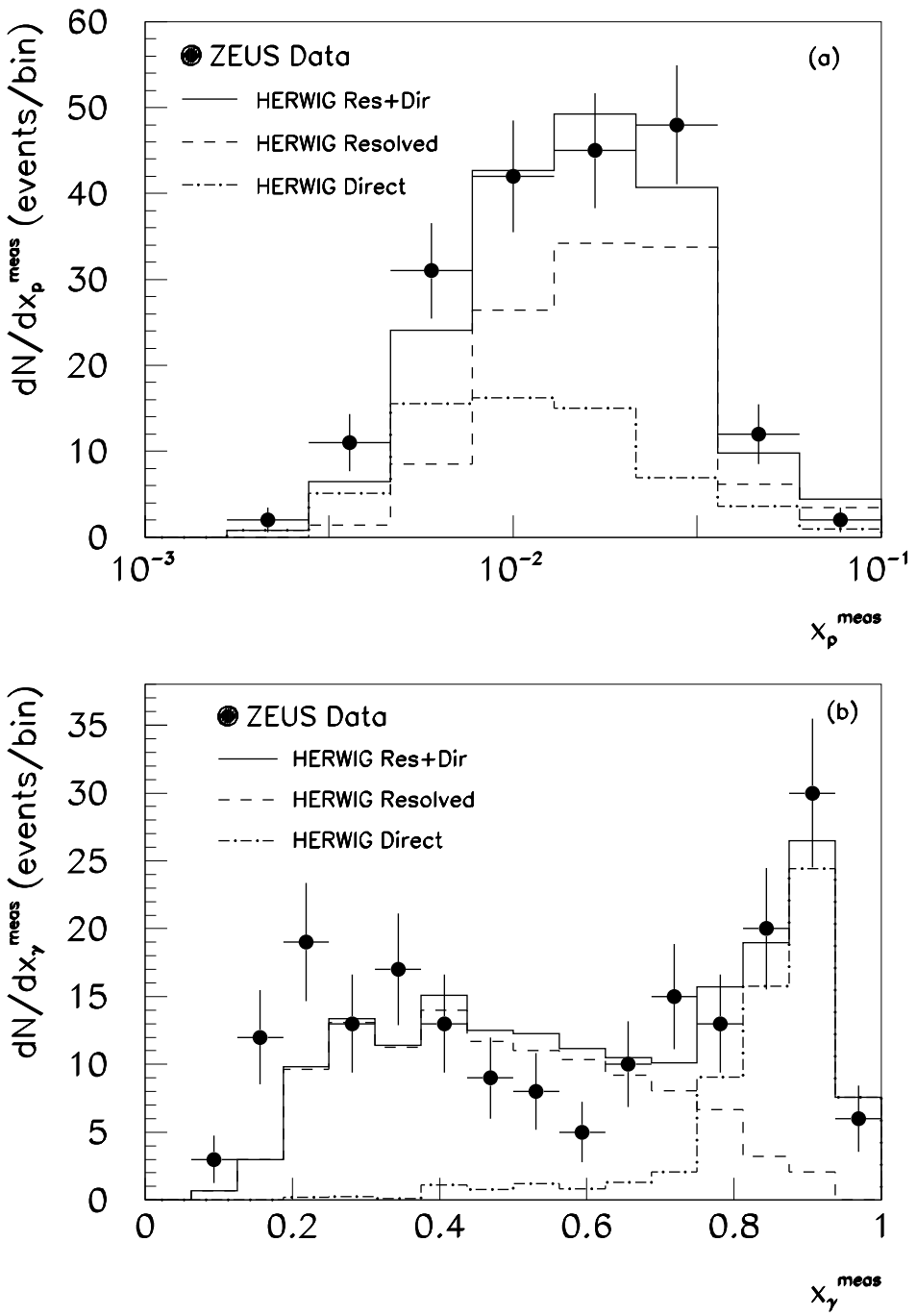

Figure 4: Kinematic distributions for events with two or more jets. (a) x_p^{meas} distribution for the final sample. (b) x_γ^{meas} distribution for the final sample. For both figures, the Monte Carlo distributions are the result of the fit to the data shown in figure 4b (see text).